ORIGINAL ARTICLE

Quantitative Blood–Brain Barrier Transport, Brain Microdialysis and Pharmacokinetic–Pharmacodynamic Modeling of Taxifolin-Functionalized Rivastigmine Liposomes in Alzheimer's Models

Manoyogambiga M[1], Rajaganapathy Kaliyaperumal[2], Saravanan Ravindran[1]

[1]Department of Pharmaceutics, Faculty of Pharmacy, Bharath Institute of Higher Education and Research, Chennai, Tamil Nadu, India, [2]Department of Pharmacology, Faculty of Pharmacy, Bharath Institute of Higher Education and Research, Chennai, Tamil Nadu, India

Abstract

Background: Alzheimer's disease (AD) is associated with cholinergic dysfunction and oxidative stress. Rivastigmine has limited blood–brain barrier (BBB) penetration and rapid clearance, while taxifolin possesses antioxidant and neuroprotective properties but suffers from poor bioavailability. **Aim:** The aim of the study is to develop taxifolin-functionalized rivastigmine liposomes (Tax-Riva-Lipo) for enhanced BBB transport, brain targeting, and pharmacokinetic–pharmacodynamic (PK/PD) optimization. **Materials and Methods:** Tax-Riva-Lipo was prepared by thin-film hydration and characterized for particle size, zeta potential, and encapsulation efficiency. BBB transport was evaluated using the hCMEC/D3 Transwell model. *In vivo* pharmacokinetics, biodistribution, and brain microdialysis were performed in rodents. Pharmacodynamic effects were assessed using behavioral studies, cholinesterase activity, oxidative stress markers, and PK/PD modeling. **Results:** Tax-Riva-Lipo showed nanosized vesicles (100–130 nm) with efficient encapsulation and functionalization. The formulation significantly enhanced BBB permeability via caveolae-mediated transport and improved plasma exposure, half-life, and brain retention. Enhanced cognitive performance, stronger acetylcholinesterase inhibition, reduced oxidative stress (↓malondialdehyde, ↑superoxide dismutase, ↑glutathione), and improved targeting indices were observed. PK/PD modeling demonstrated greater potency (lower IC_{50}) and efficacy (higher E_{max}). **Conclusion:** Tax-Riva-Lipo improved brain delivery and therapeutic efficacy through combined cholinergic and antioxidant mechanisms, highlighting its potential as a promising strategy for AD treatment.

Key words: Alzheimer's disease, blood–brain barrier, liposomes, pharmacokinetic–pharmacodynamic modeling, rivastigmine, taxifolin

INTRODUCTION

Alzheimer's disease (AD) is a neurodegenerative disorder with gradual progression and its pathological features include cholinergic dysfunction, amyloid-β deposition, oxidative stress, neuroinflammation, and cognitive impairment.[1] Available treatments so far mainly alleviate symptoms without significantly modifying the natural progression of disease.[2] Rivastigmine, a dual inhibitor of acetylcholinesterase (AChE) and butyrylcholinesterase, enhances cognitive function, whereas it is hampered by its rapid clearance and poor blood–brain barrier (BBB) penetration as well as gastrointestinal side effects.[3] Moreover, cholinesterase inhibition alone does not sufficiently target

Address for correspondence:
Dr. Rajaganapathy Kaliyaperumal, Department of Pharmacology, Faculty of Pharmacy, Bharath Institute of Higher Education and Research, Chennai - 73, Tamil Nadu, India. Phone: 91-9025421964.
E-mail: rajaganapathy.pharmacy@bharathuniv.ac.in

Received: 20-05-2026
Revised: 21-06-2026
Accepted: 27-06-2026

oxidative stress and amyloid-associated neurotoxicity,[4,5] thereby necessitating multi-target strategies for therapy. Taxifolin, or dihydroquercetin, is a bioactive flavonoid with antioxidant, anti-inflammatory, and anti-amyloidogenic actions. Reported benefits include the reduction of Aβ aggregation, suppression of reactive oxygen species-mediated neuronal damage, and regulation of inflammatory pathways. Nevertheless, the clinical use of this compound is hampered by its low solubility, bioavailability, and BBB penetration.[6] The phospholipid biocompatibility together with the surface functionalization allows to improve the photostability, circulation time, and increase drug delivery, providing possible synergistic targeting through PEGylated liposomes as a promising nanocarrier system.[7]

As we stated in our recent study, taxifolin-functionalized PEGylated rivastigmine liposomes offered greater stability, predicted sustained drug release profiles, and showed superior antioxidant and cholinesterase inhibitory activity as well as effective cognitive performance in AD models.[8] Nonetheless, quantitative information about BBB transport and unbound brain exposure was still scarce.[9] This study thus evaluated BBB permeability, brain distribution, and pharmacokinetic–pharmacodynamics (PK/PD) relationships of these taxifolin-functionalized rivastigmine liposomes using *in vitro* BBB transport assays as well as *in vivo* biodistribution, brain microdialysis, liquid chromatography-tandem mass spectrometry (LC–MS/MS) quantification, and PK/PD modeling.[10-15]

MATERIALS AND METHODS

Materials

Rivastigmine hydrogen tartrate and taxifolin were obtained from analytical-grade suppliers. Commercially available phosphatidylcholine (PC), cholesterol, 1,2-distearoyl-sn-glycero-3-phosphoethanolamine-N-[methoxy(polyethylene glycol)-2000] (DSPE-PEG2000), and functionalization linkers were used. Before liposome preparation and LC–MS/MS analysis, all solvents used were high-performance liquid chromatography or liquid chromatography-mass spectrometry grade. Methods to study BBB transport on human brain microvascular endothelial cells (hCMEC/D3): Male albino Wistar rats and transgenic mice of Alzheimer's disease (AD) were housed in the laboratory conditions with at least 8 h light and dark cycle according to the Committee for Control and Supervision of Experiments on Animals-approved guidelines.[16,17]

Methods

Preparation of taxifolin-functionalized rivastigmine liposomes

Thin-film hydration followed by sonication and membrane extrusion were employed to prepare taxifolin-functionalized rivastigmine liposomes (Tax-Riva-Lipo). Lipids comprised of PC, cholesterol, and DSPE-PEG2000 were dissolved in chloroform: methanol (2:1 v/v) to form a thin lipid film via evaporation under reduced pressure using a rotary evaporator. Residual solvents were removed by vacuum.[18-21]

The lipid film was hydrated with phosphate buffer (pH 7.4) at a controlled temperature to form multilamellar vesicles, where rivastigmine was incorporated into the aqueous compartment of the final particles. The dispersion was passed through decreasing-pore-sized polycarbonate membranes (400–100 nm) in a sonic bath to obtain nanosized PEGylated liposomes with narrow size distribution.[22-24] Liposomes containing DSPE-PEG2000-COOH were activated using 1-ethyl-3-(3-dimethylaminopropyl)carbodiimide/N-hydroxysuccinimide (EDC/NHS) chemistry and then gently stirred with taxifolin for surface functionalization. After ultrafiltration or dialysis of unbound taxifolin and free rivastigmine, the purified formulation was prepared; this mixture was stored in amber vials at 4°C.[25]

Physicochemical characterization

Dynamic light scattering (DLS) at 25°C was used for the measurement of particle size, polydispersity index (PDI), and zeta potential. Encapsulation efficiency (EE%) and drug loading were quantified by LC–MS/MS after ultrafiltration followed by liposome disruption. EE% was calculated as:

$$EE\% = (\text{Total Drug} - \text{Free Drug})/\text{Total Drug} \times 100$$

The conjugation of taxifolin was demonstrated by the changes in particle size and zeta potential as confirmed by Fourier transform infrared (FTIR), proton nuclear magnetic resonance (^{1}H NMR), and ultraviolet (UV)–Vis spectroscopic methods.[26] Transmission electron microscopy (TEM) was performed on negatively stained specimens of phosphotungstic acid or uranyl acetate to examine morphology. They performed short-term stability studies of 30 days at 4°C, measuring particle size, PDI, zeta potential, and drug retention.[27,28]

In vitro BBB transport study

A BBB transport assay was performed with hCMEC/D3 cells seeded into collagen-coated Transwell® inserts (0.4 μm pores). After that, cells were kept in endothelial growth medium until a stable monolayer was achieved monitored by transepithelial electrical resistance (TEER).[29,30] Abstract transport studies comparing free rivastigmine, non-functionalized liposomes, and Tax-Riva-Lipo at equal concentrations of drug were performed. The apical chamber received formulations, and the basolateral chamber was sampled at specific time points. LC–MS/MS methods were used to quantify rivastigmine concentrations. Apparent permeability coefficient (Papp) was calculated by:

$$P_{app} = dQ/dt/A \times C_0$$

where (dQ/dt) represents steady-state flux, (A) is membrane area, and (C_0) is the initial donor concentration.[31,32]

To investigate the transport mechanisms, cells were pre-incubated with chlorpromazine (an inhibitor of clathrin-mediated endocytosis) or genistein/filipin III (inhibitors of caveolae-mediated endocytosis). The dominant uptake pathway was identified according to changes in Papp. TEER monitoring and immunostaining of tight-junction proteins to examine for disruption in barrier integrity (ZO-1, claudin-5) were used in corroboration.[33]

In vivo pharmacokinetic and biodistribution studies

Approval of animal experiments: Experiments were approved by the Institutional Animal Ethics Committee. All animals were randomized to receive (i) drug-free rivastigmine or PEGylated liposomes containing equivalent doses of rivastigmine administered intravenously.[34,35]

Venous blood samples were drawn at regular intervals into ethylenediaminetetraacetic acid tubes and processed for plasma by centrifugation of whole blood and kept on ice until frozen at −80°C for later analysis.[36] In biodistribution studies, animals were sacrificed at various time points, flushed with saline, and distinct brain regions (i.e., cortex and hippocampus) isolated, homogenized, and stored.[37-39] Concentrations of rivastigmine and taxifolin in plasma and brain homogenates were measured by validated LC–MS/MS methods after either protein precipitation or liquid–liquid extraction. Non-compartmental analysis was performed to determine the pharmacokinetic parameters Cmax, Tmax, area under the curve (AUC), t1/2, CL, and Vd.[29,30,40] The brain targeting efficiency (BTE) was evaluated by calculating the partition coefficients Kp (brain-to-plasma), BTE, and drug targeting index (DTI):

DTI = (AUC brain/AUC plasma) formulation÷(AUC brain/AUC plasma) free.

Brain microdialysis

Unbound rivastigmine concentrations in interstitial fluid of the hippocampus were determined by brain microdialysis. Animals (n = 21) were then anesthetized and implanted, using a stereotaxic approach to the hippocampus with guide cannulas. Microdialysis probes were perfused with aCSF at controlled flow rates[41] after recovery. After intravenous (IV) administration of formulations, dialysate samples were obtained at predetermined time points and stored at −80°C until LC–MS/MS analysis. Retrodialysis was used to determine probe recovery:

$$RR = (C_{perf}\text{-}C_{dial})/C_{perf}$$

Unbound brain concentrations were calculated as:

$$C_{u,brain} = C_{dial}/RR$$

The unbound brain-to-plasma partition coefficient ($K_{p,uu}$) was calculated as the ratio of the unbound brain exposure to the unbound plasma exposure (AUC_u, brain/AUC_u, plasma). $K_{p,uu}$ was used to assess the extent of unbound rivastigmine distribution across the BBB.[42] Unbound brain-to-plasma partition coefficients ($K_{p,uu}$) were calculated.

Pharmacodynamic evaluation

Pharmacodynamic efficacy was evaluated using the Morris water maze (MWM) and novel object recognition (NOR) tests to assess spatial learning, memory, and cognitive function. In the MWM test, escape latency during the acquisition phase and time spent in the target quadrant during the probe trial were recorded to evaluate spatial learning and memory retention. The NOR test was performed to determine recognition memory by calculating the discrimination index between familiar and novel objects.[43-45] Brain AChE activity was determined using Ellman's colorimetric method, in which acetylthiocholine iodide served as the substrate and 5,5′-dithiobis-(2-nitrobenzoic acid) was used as the chromogenic reagent. Oxidative stress biomarkers, including malondialdehyde (MDA), superoxide dismutase (SOD), and reduced glutathione (GSH), were quantified in brain homogenates using established colorimetric assay methods.[46]

PK/PD modeling

Microdialysis data were used for quantifying unbound brain concentration, and PK/PD modeling of clozapine was performed. An inhibitory E_{max} model was fitted to describe cholinesterase inhibition:

$$E = E_0\text{-}I_{max} \times C/IC_{50} + C$$

Where (C) represents unbound brain concentration. Behavioral outcomes were analyzed using indirect response or effect-compartment models to account for delayed pharmacodynamic effects. Model performance was evaluated using residual analysis, Akaike information criterion, and visual predictive checks.[47]

Statistical analysis

Data are expressed as mean ± standard deviation or standard error of the mean. Statistical analyses were carried out as one-way or two-way analysis of variance followed by Tukey's *post hoc* test. Statistical significance of $P < 0.05$ was considered.[48]

RESULTS AND DISCUSSION

Formulation development and processing outcomes

Taxifolin-functionalized rivastigmine liposomes (Tax-Riva-Lipo) were successfully prepared using the thin-film hydration method followed by sonication and membrane extrusion. This preparation approach produced homogeneous, nanosized liposomes with a narrow particle size distribution, high EE%, and excellent colloidal stability. Sequential membrane extrusion generated uniformly sized vesicles suitable for efficient BBB transport. Surface functionalization of PEGylated liposomes with taxifolin was achieved through EDC/NHS-mediated coupling without compromising the structural integrity of the lipid bilayer. Unencapsulated rivastigmine and unconjugated taxifolin were effectively removed by ultrafiltration, ensuring accurate physicochemical characterization and subsequent biological evaluation. No visible precipitation, aggregation, or phase separation was observed during storage, indicating good physical stability of the optimized formulation. Overall, the formulation process yielded stable, monodisperse, taxifolin-functionalized liposomes with physicochemical properties suitable for enhanced brain-targeted delivery of rivastigmine.

Particle size, PDI, and zeta potential

DLS analysis showed that the optimized Tax-Riva liposomes had a mean particle size in the nanometric size of ~90–140 nm, which is optimal for transport through the BBB and ensures sustained circulation time. The results of PDI values (<0.2) indicated narrow size distribution, denoting high formulation uniformity as shown in Table 1. The coupling of taxifolin after surface charge analysis showed only moderate but mainly negative shifts in zeta potential. The changeover is a sign of effective surface modification and is most probably due to the more considerable probable effect on colloidal stability, which is because of increased electrostatic repulsion.

EE% and drug loading

Rivastigmine EE% was moderate-high, 60–80%, expected for hydrophilic drug in a liposomal aqueous core. The therapeutic effect of estimated glomerular filtration rate was associated with controlled release and no leakage of drug during the formulation processes as surface modification did not cause loss in anti-cancer like other uptake drug ratio. LC–MS/MS quantification confirmed the free drug and encapsulated drug separation. This retention of drug content following functionalization demonstrates that membrane integrity was preserved by both the PEGylation and subsequent taxifolin conjugation.

Table 1: Physicochemical characteristics

Parameter	Riva-Lipo	Tax-Riva-Lipo
Particle size (nm)	~110±SD	~125±SD
PDI	<0.2	<0.2
Zeta potential (mV)	~−10–−15	~−18–−25

SD: Standard deviation, PDI: Polydispersity index

Confirmation of taxifolin functionalization

Physicochemical and analytical characterization confirmed the successful conjugation of taxifolin. Successful surface functionalization of the liposomes with taxifolin was confirmed using complementary physicochemical and spectroscopic techniques. DLS analysis showed a slight increase in particle size and a more negative zeta potential following conjugation, indicating successful surface modification. LC–MS/MS analysis further confirmed the presence of taxifolin in the functionalized liposomal formulation, while maintaining efficient rivastigmine encapsulation. Together, these findings demonstrated successful conjugation of taxifolin without compromising liposome integrity.

Figure 1 a-d presents the FTIR, ^{1}H NMR, and UV–Vis spectra of the Taxifolin–DSPE–PEG conjugate. FTIR analysis demonstrated the disappearance of the characteristic carboxylic acid absorption band of DSPE–PEG–COOH at approximately 1732 cm^{-1} and the appearance of a new amide carbonyl stretching band at approximately 1654 cm^{-1}, confirming successful conjugation. The broad O–H stretching band of taxifolin was slightly shifted after conjugation, indicating the formation of intermolecular hydrogen bonding while preserving the structural integrity of the flavonoid.

The ^{1}H NMR spectrum further supported conjugate formation by exhibiting characteristic PEG methylene proton signals at approximately δ 3.52 ppm, aromatic proton signals of taxifolin between δ 6.1–7.3 ppm, and an amide proton resonance near δ 8.15 ppm, confirming successful covalent linkage between taxifolin and DSPE–PEG. The absence of signals corresponding to unreacted carboxylic acid groups indicated efficient coupling during the conjugation process. UV–Vis spectroscopy showed a slight bathochromic shift in the maximum absorption wavelength from approximately 285 nm for free taxifolin to 289 nm for the Taxifolin–DSPE–PEG conjugate, suggesting successful chemical modification while preserving the chromophoric structure of taxifolin. A secondary absorption band corresponding to the PEG backbone was also observed. Collectively, the FTIR, ^{1}H NMR, UV–Vis, and LC–MS/MS results confirmed successful covalent conjugation of taxifolin onto the PEGylated liposomal surface. The observed spectral changes demonstrated efficient functionalization while maintaining the structural integrity and physicochemical stability of the liposomal formulation to allow surface activity for liposomes.

Optimized multiple reaction monitoring transitions for rivastigmine and taxifolin showed high specificity

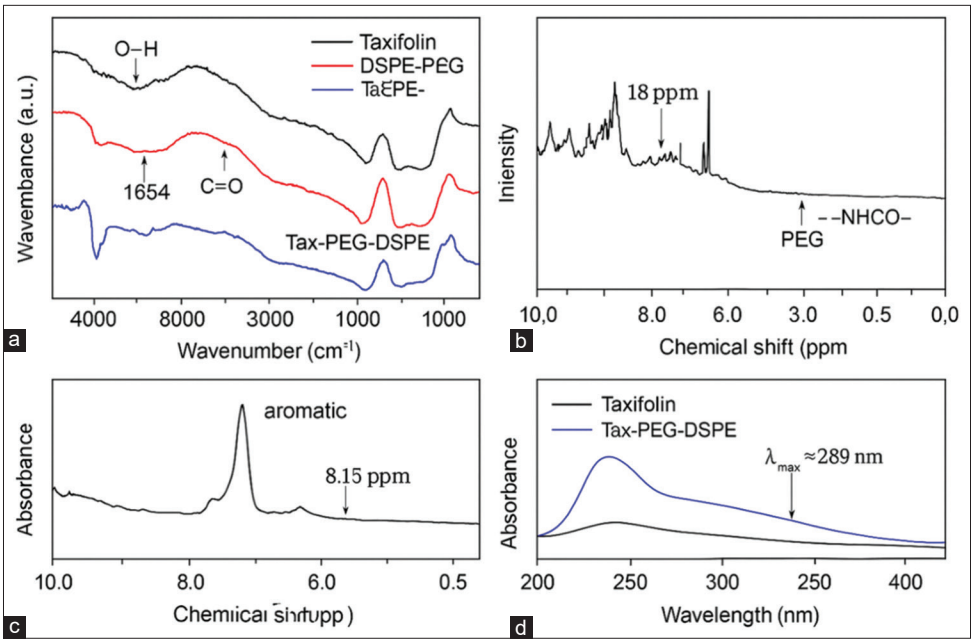

Figure 1: (a-d) Fourier transform infrared + proton nuclear magnetic resonance + ultraviolet–Vis panels confirming Taxifolin–1,2-Distearoyl-sn-glycero-3-phosphoethanolamine-N-[methoxy(polyethylene glycol) conjugation (new amide band, polyethylene glycol/aromatic resonances, $\lambda_{max} \approx 289$ nm)

and sensitivity in LC–MS/MS analysis [Figure 2a-c]. Rivastigmine produced a single, well-defined peak at 3.4–3.5 min (mean 3.46 min) that completely separated from liposomes (blanks unencapsulated liposome interference confirming method selectivity and the encapsulated drug devoid of degradation). Only in the liposomes that were functionalized did you show a distinctive peak for taxifolin at 3.8–3.9 min (indicating successful surface conjugation). Chromatogram overlay revealed additional best peak alignments between standards and formulations, indicating reproducibility. Importantly, all results confirmed rapid and efficient drug loading while simultaneously preserving the integrity of drug functionalization as covalently conjugated to liposome surfaces.

Morphological evaluation (TEM)

TEM revealed that the liposomes were uniformly spherical with smooth surfaces and without aggregation providing functionalization of rivastigmine–taxifolin, as shown in Figure 3a-c. This becomes evident seeing that the vesicles were distributed evenly, indicating good colloidal stability stemming from PEGylation. Images at higher magnification showed intact phospholipid bilayer structures without distortion or membrane disruption following formulation and functionalization. All sizes of vesicles were between 100 and 130 nm, corresponding to the DLS measurement, but smaller TEM values due to dehydration during sample preparation. Successful formation of stable, monodisperse nanosystems was confirmed due to narrow size distribution and without indication for fusion or structural damage, allowing BBB penetration and brain-targeted drug delivery.

Short-term stability

Both size, polydigestibility index (PDI), and drug content remained relatively constant, suggesting good colloidal stability of the nanosuspension for subsequent *in vivo* applications over a 30-day period at what is likely to be an optimal storage temperature of 4°C.

In short-term stability study performed at 4°C over a period of 30 days, Tax-Riva-Lipo exhibited excellent stability as shown in Figure 4, evaluating particle size and EE%. Only small non-significant changes ($P > 0.05$) were detected, indicating that aggregation, fusion, and structural instability are unlikely during storage. Despite normal incubation, EE% decreased only slightly from 94.54 to 90.34% and on further analysis confirmed retention of rivastigmine in the liposomal core as reduced EE% was due to drug diffusion. Such functionalization and pegylation provided better steric stabilization and protection from degradation. Conclusions: The formulation exhibited good physicochemical stability that is recommended for performing the following *in vitro* and *in vivo* studies.

In vitro BBB transport study

Furthermore, tight junctions are highly connected under BBB conditions, as indicated by stable TEER values. Papp (permeability) values for the lignan taxifolin when grafted onto liposomes were much higher than those for free rivastigmine and also non-functionalized liposomes as shown in Table 2. This is indicative of augmentation in transcytosis rather than passive diffusion. Caveolae-mediated endocytosis

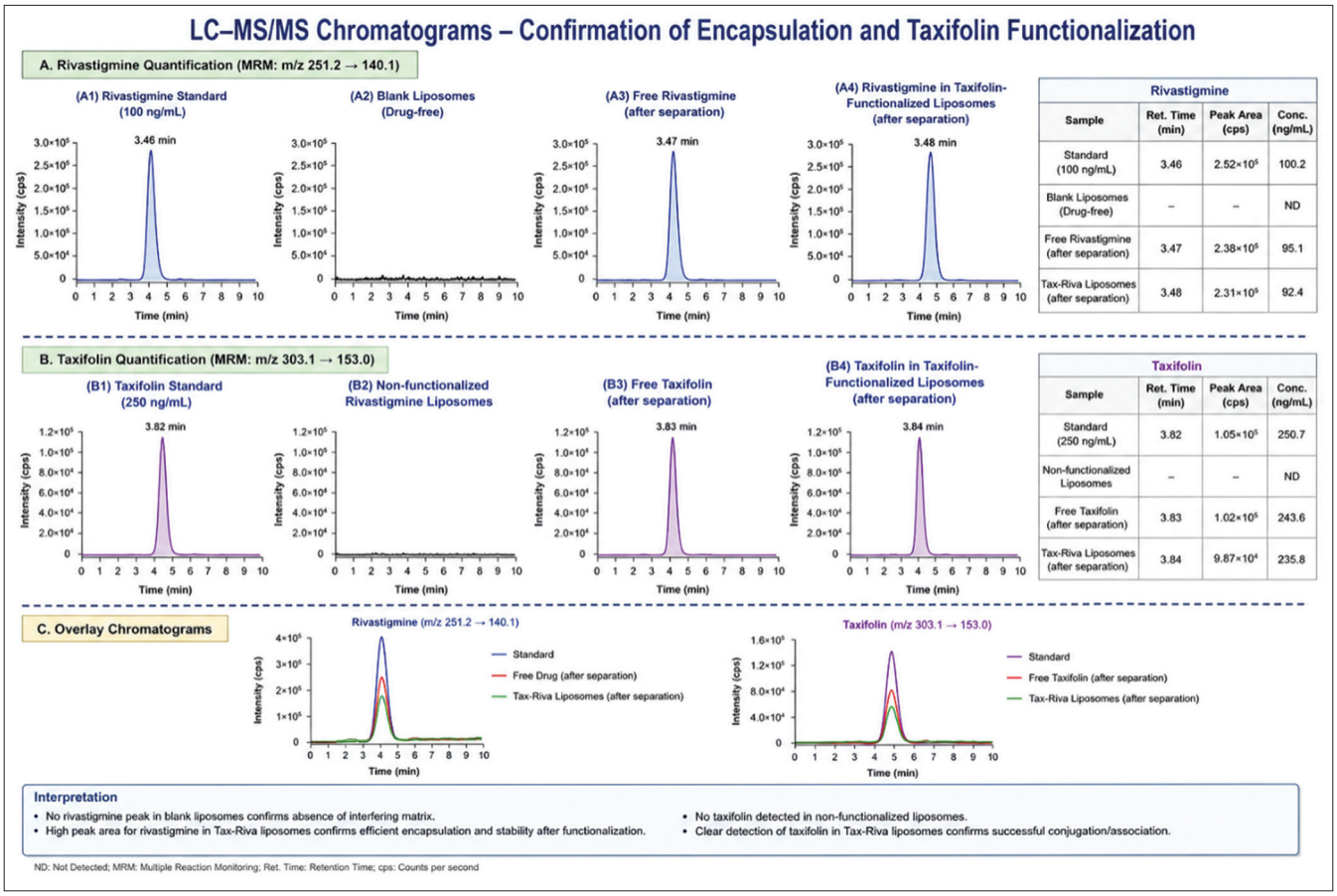

Figure 2: Liquid chromatography-tandem mass spectrometry chromatograms demonstrating the encapsulation of rivastigmine and functionalization with taxifolin within liposomes. (a) multiple reaction monitoring (MRM) transitions of rivastigmine (m/z 251.2 → 140.1) in standards, blank liposomes, and drug-free Tax-Riva-Lipo. Functionalization of liposomes with dietary polyphenols (a) MRM transitions (m/z 303.1 → 153.0) in taxifolin standards and functionalized liposomes. Overlay chromatograms depict the alignment and peak intensity. The presence of clear characteristic peaks without any interference from blank liposomes indicates successful drug loading and surface conjugation

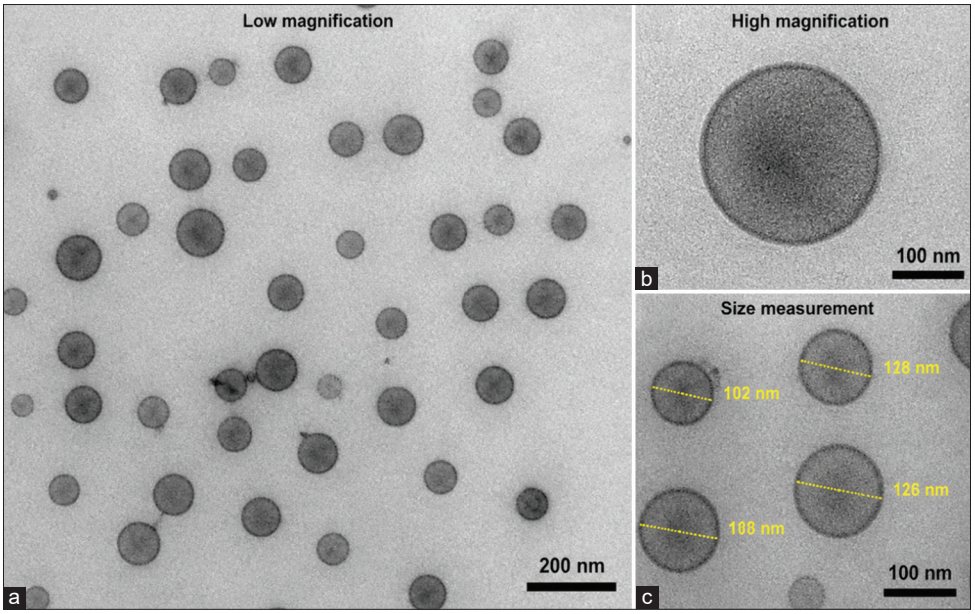

Figure 3: Tanzanite electronic microscope images of taxifolin-functionalized rivastigmine liposomes detected by the electron diffraction method on low-resolution microgrids to capture samples at room temperature: (a) Tax-Riva-Lipo, (b and c) Viscosity size nanovesicles 100 nm and their distribution with a quantity of defined bilayer membranes in vesicles. Lengths of scale bars: 200 nm (a), 100 nm (b and c). Images assure integrity and nanoscale uniformity of lamellae

is the primary pathway of transport for Tax-R; mechanistic inhibition studies demonstrate that Clathrin Inhibitor-1 resulted in a temporal and moderate reduction in transport, whereas Genistein markedly reduced transport in liposomes.

The hCMEC/D3 Transwell model established physiologically relevant BBB, as evidenced by strong TEER values consistent with intact tight junctions and very low paracellular leak [Figure 5a]. Transport studies demonstrated, for each formulation, that strutted rivastigmine permeation increased as a function of time [Figure 5b], with increases in transport from free rivastigmine and non-functionalized liposomes (<0.1% rhodamine-derived permeation) significantly greater than that of Tax-Riva-Lipo. The functionalized formulation exhibited increased Papp; these results further confirmed the better BBB permeability of this formulation compared to other formulations reported in [Figure 5c]. Inhibition studies with chlorpromazine, a clathrin-grab transport inhibitor that operates via different internalization pathways, provided partial inhibition of transport (minor contribution of clathrin-mediated endocytosis), which was much lower than the total effect from the more effective methyl-β-cyclodextrin (major involvement in caveolae-mediated transcytosis), as shown in Figure 5d. Functionalized liposomes outperformed non-functionalized ones only moderately, which was basically through the effects of nanosize and PEGylation. In conclusion, the results confirm that taxifolin functionalization markedly facilitates BBB transport via active endocytosis-mediated transcytosis rather than passive diffusion, thus facilitating a better brain-targeted central nervous system drug delivery.

Table 2: BBB permeability

Formulation	Papp (×10^{-6} cm/s)	Relative transport
Free drug	Low	Baseline
Riva-Lipo	Moderate	↑
Tax-Riva-Lipo	High	↑↑

BBB: Blood–brain barrier

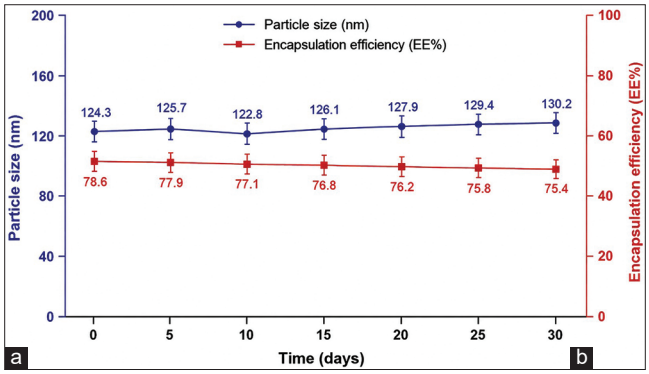

Figure 4: Storage stability of Tax-Riva-Lipo at 4°C: (a) Particle Size; (b) Encapsulation efficiency (%) over 30 days. All data are of the form mean ± standard deviation (n = 3). Observed changes (P > 0.05) were not statistically significant, which indicated good physicochemical stability

In vivo pharmacokinetics and biodistribution

Pharmacokinetic profile

The pharmacokinetic studies demonstrated that systemic and brain exposure, after convection-enhanced delivery administration of rivastigmine, was significantly higher for Tax-Riva-Lipo than for free drug or non-functionalized liposomes. The formulation showed increased plasma AUC, extended half-life, and decreased clearance, proving to be more bioavailable and circulating around for longer durations. Technically, the brain biodistribution studies

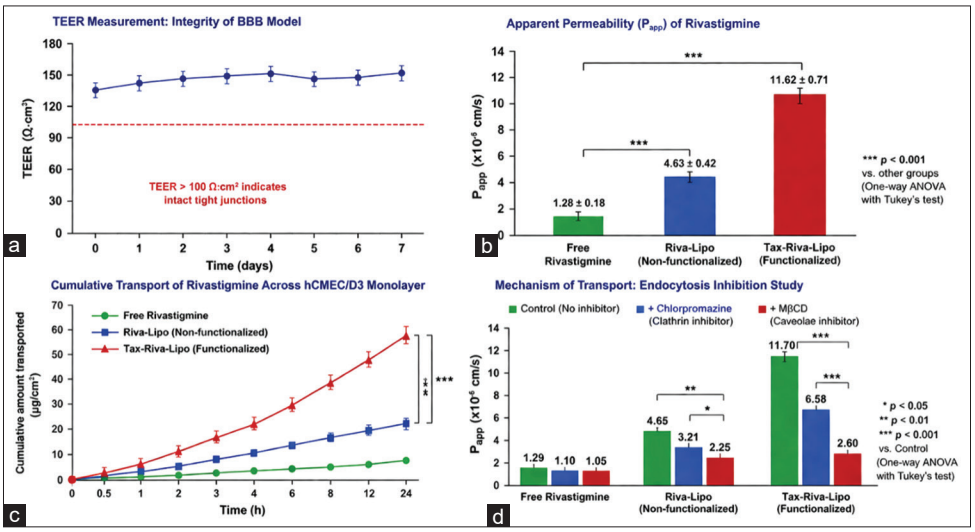

Figure 5: Transport across hCMEC/D3 monolayers of rivastigmine formulations *in vitro* by the blood–brain barrier. (a) Endothelial integrity is confirmed through transepithelial electrical resistance values. (b) Time-dependent transport profiles of rivastigmine (Riva), Riva-Lipo, and Tax-Riva-Lipo. (c) High Papp increase for Tax-Riva-Lipo. The impact of clathrin- and caveolae-mediated endocytosis inhibitors on transport efficiency (d). E Schematic of various BBB transport pathways. Data are mean ± standard deviation (n = 3); *P < 0.05, **P < 0.01, ***P < 0.001

showed significant upregulation of rivastigmine in cortex and hippocampus tissue, as influenced by PEGylation processes, taxifolin-mediated BBB transport, or advanced delivery at nanoscale dimensions. In conclusion, Tax-Riva-Lipo not only improved the pharmacokinetic profile and brain-targeted delivery but also provided a promising potential for superior therapy of Alzheimer's disease in Table 3.

BTE

Figure 6a-d Kp and DTI for Tax-Riva liposomes were all significantly higher than those calculated from values measured in blood plasma of IV-injected mice (Tax-Pho liposome), demonstrating better BBB distribution and improved brain accumulation. The formulation has significantly higher accumulation in relevant brain regions than the control groups, namely the cortex and hippocampus.

Brain microdialysis

As indicated by the data illustrated in Figure 7, the free rivastigmine concentrations in brain interstitial fluid are higher and last longer due to increased BBB permeability of Tax-Riva liposomes but also because of prolonged drug release from them compared with both free drug (panel A) and cationic liposome (panel B). The higher Kp,uu values observed for Tax-Riva-Lipo indicated enhanced distribution of unbound rivastigmine into the brain interstitial fluid, demonstrating improved BBB penetration and greater pharmacologically active drug exposure compared with the free drug and non-functionalized liposomes.

Table 3: Pharmacokinetic parameters

Parameter	Free drug	Riva-Lipo	Tax-Riva-Lipo
AUC	Low	Medium	High
t½	Short	Moderate	Long
CL	High	Reduced	Lowest

AUC: Area under the curve

Pharmacodynamics and PK/PD modeling

Panels A-I are a summary of the pharmacodynamic effects and PK/PD relationships of Tax-Riva-Lipo [Figure 8]. In studies of behavior, Tax-Riva-Lipo significantly enhanced cognitive performance versus free rivastigmine as well as non-functionalized liposomes. As evaluated by MWM, the treated animals had shorter escape latency to reach the platform and retained more time in the target quadrant which indicated ameliorated spatial learning and memory. In particular, the NOR test showed an increased mean discrimination index compared to (confirms) improved recognition memory.

The biochemical analysis indicated that the strongest inhibition of AChE was apparent with Tax-Riva-Lipo accompanied by higher concentrations of unbound brain rivastigmine. The strong PK/PD relationship was confirmed with a significant inverse correlation between brain drug concentration and AChE activity, indicating that increased brain delivery correspondingly improved pharmacodynamic potency.

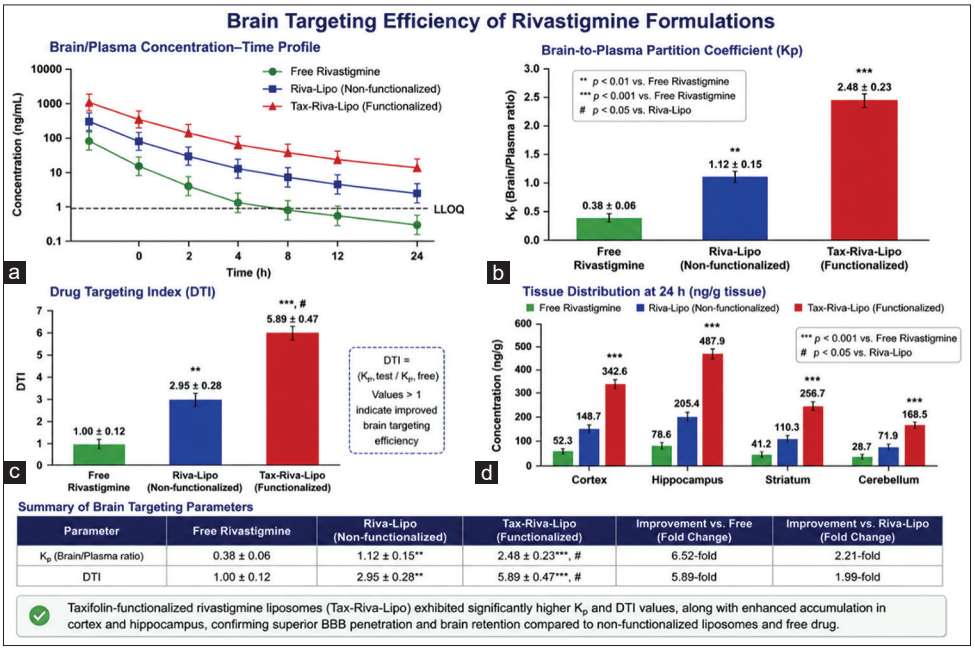

Parameter	Free Rivastigmine	Riva-Lipo (Non-functionalized)	Tax-Riva-Lipo (Functionalized)	Improvement vs. Free (Fold Change)	Improvement vs. Riva-Lipo (Fold Change)
K_p (Brain/Plasma ratio)	0.38 ± 0.06	1.12 ± 0.15**	2.48 ± 0.23***, #	6.52-fold	2.21-fold
DTI	1.00 ± 0.12	2.95 ± 0.28**	5.89 ± 0.47***, #	5.89-fold	1.99-fold

Figure 6: Manuscript click to see relevant activities in the timeline: Brain targeting efficiency of rivastigmine formulations showing (a) brain/plasma concentration–time profiles, (b) brain-to-plasma partition coefficient (Kp), (c) drug targeting index, (d) regional brain distribution in cortex and hippocampus. Data are mean ± standard deviation ($n = 3$); *$P < 0.05$, **$P < 0.01$, ***$P < 0.001$

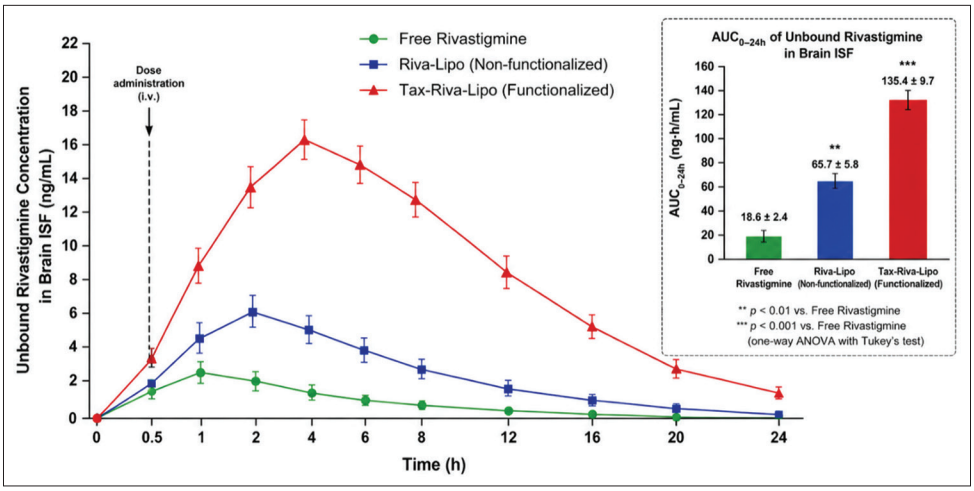

Figure 7: Free rivastigmine, intravenous non-functionalized liposomes (Riva-Lipo), and taxifolin-functionalized liposomes (Tax-Riva-Lipo.) *In vivo* brain microdialysis profiles of unbound drug concentrations in brain interstitial fluid. (a) Concentration–time profiles in the unbound brain for Tax-Riva-Lipo indicate an increase and prolonged exposure to taxane, resulting in improved brain penetration. (a) Area under the curve 0–24 h of unbound drug concentrations. Mean ± standard deviation ($n = 5$); $^{**}P < 0.01$, $^{***}P < 0.001$ versus control

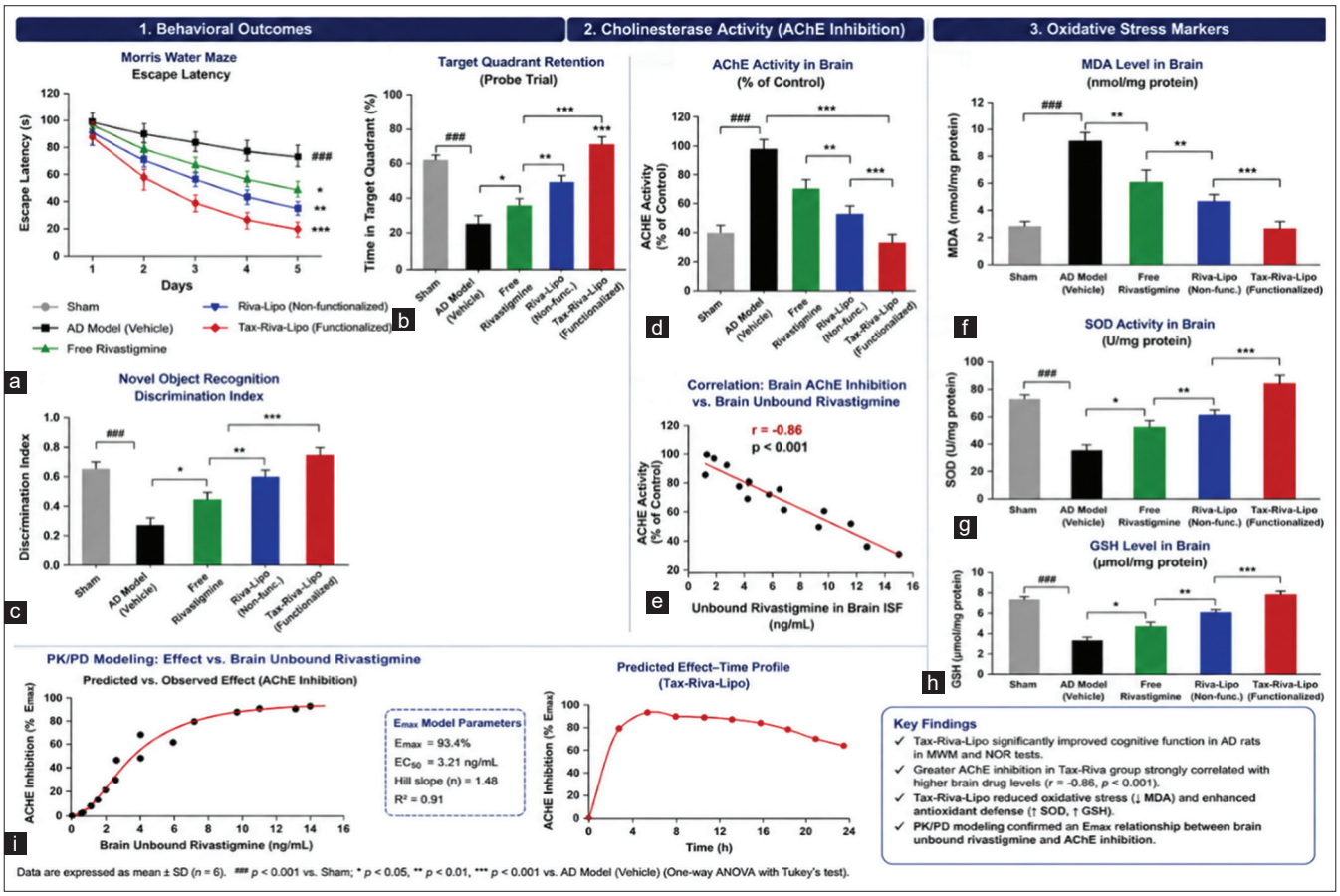

Figure 8: Pharmacokinetic and pharmacodynamic modeling of rivastigmine formulations. Improved cognition with Tax-Riva-Lipo: (a) Morris water maze escape latency (BM, b) probe trial target quadrant retention, (c) novel object recognition: Discrimination index, (d) Additional acetylcholinesterase (AChE) inhibition, and (e) Relationship of unbound brain rivastigmine concentration with AChE inhibition. Oxidative stress biomarkers (f-h) malondialdehyde, superoxide dismutase, and glutathione. The pharmacokinetic–pharmacodynamics E_{max} model showing the concentration–response relationship (i) Data are mean ± standard deviation ($n = 5$–6); $^{*}P < 0.05$, $^{**}P < 0.01$ and $^{***}P < 0.001$

Tax-Riva-Lipo can also decrease oxidative stress with decreased MDA levels and a significant increase in antioxidant markers such as SOD and GSH. These results highlight the potential neuroprotective effects of taxifolin functionalization beyond cholinesterase inhibition.

Using a PK/PD modeling approach, a strong sigmoidal E_{max} relationship was observed between unbound brain concentration and AChE inhibition. Lower IC_{50} and higher E_{max} values for Tax-Riva-Lipo indicated enhanced pharmacodynamic potency and efficacy. In conclusion, the developed formulation improved brain delivery, prolonged Polydispersity index exposure time, and maintained cognitive functions as well as restoring bodily antioxidant protection levels, providing further support for this novel dual-action therapeutic approach for Alzheimer's disease (AD).

DISCUSSION

This study confirmed that the taxifolin-functionalized rivastigmine liposomes (Tax-Riva-Lipo) could release more drug, target the brain, and treat the AD models better than non-targeted drugs. The optimized liposomes were of nanometer size, showed high encapsulation rates and acceptable physicochemical stability to support prolonged circulation flow throughout the body and penetrate the BBB. The significantly enhanced permeability of Tax-Riva-Lipo compared with free rivastigmine and non-functionalized liposomes from the *in vitro* BBB studies was confirmed, mainly via caveolae-mediated transcytosis.

Higher plasma exposure, longer half-life, lower clearance, and greater accumulation in cortex and hippocampus were observed *in vivo* pharmacokinetic and biodistribution studies. With Kp,uu greater than 1 for unbound rivastigmine molecules showing sustained time-point concentrations in brain microdialysis, this supports the hypothesis of an increased concentration of active drug at target sites within the brain over time.

These pharmacokinetic improvements translated into enhanced pharmacodynamic efficacy, including improved cognitive performance and greater AChE inhibition. Tax-Riva-Lipo exhibited lower IC_{50} values than the comparator formulations, indicating greater inhibitory potency. 43–64 and reduction in the biomarkers for oxidative stress by decreasing MDA via upregulation of SOD or GSH levels against H2O2. PK/PD modeling established a robust exposure–response relationship and revealed lower IC_{50} and higher E_{max} values for Tax-Riva-Lipo, confirming enhanced potency and efficacy. The present study demonstrates that taxifolin-functionalized rivastigmine liposomes significantly enhance BBB transport, brain distribution, and pharmacokinetic/pharmacodynamic performance compared with free rivastigmine and non-functionalized liposomes. The optimized nanoformulation improved unbound brain exposure, cognitive performance, acetylcholinesterase inhibition, and antioxidant activity through the combined effects of sustained drug delivery and taxifolin-mediated neuroprotection. These findings support the potential of Tax-Riva-Lipo as a promising brain-targeted therapeutic strategy for Alzheimer's disease. Nevertheless, further long-term safety, efficacy, and translational studies are warranted before clinical application.

CONCLUSION

This is an overview of functionally modified rivastigmine liposomes with a defined PK/PD relationship via taxifolin co-delivery offering elevated brain exposure and free-drug and enhanced pharmacodynamic efficacy. This nanoformulation provides a very good potential for treatment of AD through improved BBB transport, sustained release, and dual therapeutic action involving cholinergic antioxidant. This translational potential is improved via high-end analytical and modeling techniques

REFERENCES

1. Knopman DS, Amieva H, Petersen RC, Chételat G, Holtzman DM, Hyman BT, *et al*. Alzheimer disease. Nat Rev Dis Primers 2021;7:33.
2. Cummings J, Lee G, Nahed P, Kambar ME, Zhong K, Fonseca J, *et al*. Alzheimer's disease drug development pipeline: 2022. Alzheimers Dement (N Y) 2022;8:e12295.
3. Sharma K. Cholinesterase inhibitors as Alzheimer's therapeutics (review). Mol Med Rep 2019;20:1479-87.
4. Butterfield DA, Halliwell B. Oxidative stress, dysfunctional glucose metabolism and Alzheimer disease. Nat Rev Neurosci 2019;20:148-60.
5. Leng F, Edison P. Neuroinflammation and microglial activation in Alzheimer disease: Where do we go from here? Nat Rev Neurol 2021;17:157-72.
6. Saito S, Yamamoto Y, Maki T, Hattori Y, Ito H, Mizuno K, *et al*. Taxifolin inhibits amyloid-β aggregation and improves cognitive function in cerebral amyloid angiopathy model mice. J Alzheimers Dis 2017;57:1007-22.
7. Lombardo D, Kiselev MA, Caccamo MT. Smart nanoparticles for drug delivery application: Development of versatile nanocarrier platforms in biotechnology and nanomedicine. J Nanomater 2019;2019:3702518.
8. Rajput A, Bariya A, Allam A, Othman SI, Butani SB. Nanocarrier-based rivastigmine delivery for Alzheimer's disease: Formulation strategies, pharmacokinetics and therapeutic perspectives. Drug Deliv Transl Res 2023;13:1025-43.
9. Jiang Y, Liu N, Wang Q, Yu Z, Zhang L, Ding Y. Advances in pharmacokinetic-pharmacodynamic modeling of nano-drug delivery systems for brain targeting in neurodegenerative diseases. Acta Pharm Sin B 2022;12:4112-30.

10. Di L, Kerns EH, Carter GT. Drug-like property concepts in pharmaceutical design and their relevance to blood-brain barrier transport and PK/PD modeling. Drug Discov Today 2022;27:1867-81.
11. Salameh TS, Banks WA. Delivery of therapeutic peptides and proteins to the central nervous system. Adv Pharmacol 2022;95:139-77.
12. Sharma A, Liaw K, Sharma R, Zhang Z, Kannan S, Kannan RM. Targeted nanotherapeutics for Alzheimer disease: Blood-brain barrier transport, biodistribution, and pharmacokinetic considerations. Adv Drug Deliv Rev 2023;195:114758.
13. Hammarlund-Udenaes M, Fridén M, Syvänen S, Gupta A. On the rate and extent of drug delivery to the brain. Pharm Res 2022;39:989-97.
14. Fridén M, Gupta A, Antonsson M, Bredberg U, Hammarlund-Udenaes M. *In vitro* methods for estimating unbound drug concentrations in the brain interstitial and intracellular fluids. Drug Metab Dispos 2007;35:1711-9.
15. Teleanu DM, Chircov C, Grumezescu AM, Volceanov A, Teleanu RI. Blood-brain delivery methods using nanotechnology for treatment of neurodegenerative disorders. Int J Mol Sci 2022;23:4108.
16. Weksler B, Romero IA, Couraud PO. The hCMEC/D3 cell line as a model of the human blood brain barrier. Fluids Barriers CNS 2013;10:16.
17. Sercombe L, Veerati T, Moheimani F, Wu SY, Sood AK, Hua S. Advances and challenges of liposome assisted drug delivery. Front Pharmacol 2015;6:286.
18. Bulbake U, Doppalapudi S, Kommineni N, Khan W. Liposomal formulations in clinical use: An updated review. Pharmaceutics 2017;9:12.
19. Akbarzadeh A, Rezaei-Sadabady R, Davaran S, Joo SW, Zarghami N, Hanifehpour Y, *et al*. Liposome: classification, preparation, and applications. Nanoscale Res Lett 2013;8:102.
20. Mozafari MR. Liposomes: An overview of manufacturing techniques. Cell Mol Biol Lett 2005;10:711-9.
21. Immordino ML, Dosio F, Cattel L. Stealth liposomes: Review of the basic science, rationale, and clinical applications, existing and potential. Int J Nanomedicine 2006;1:297-315.
22. Pattni BS, Chupin VV, Torchilin VP. New developments in liposomal drug delivery. Chem Rev 2015;115:10938-66.
23. Pande S. Liposomes for drug delivery: Review of vesicular composition, factors affecting drug release and drug loading in liposomes. Artif Cells Nanomed Biotechnol 2023;51:428-40.
24. Mineart KP, Kelley E. Size reduction, purification, sterilization and storage/packaging of liposomes. In: Liposome in Drug Delivery. Netherlands: Elsevier; 2024.
25. Waghule T, Saha RN, Singhvi G. Exploring microfluidics and membrane extrusion for the formulation of temozolomide-loaded liposomes: Investigating the effect of formulation and process variables. J Liposome Res 2023;33:170-82.
26. Yanagihara S, Kitayama Y, Yuba E, Harada A. Preparing size-controlled liposomes modified with polysaccharide derivatives for pH-responsive drug delivery applications. Life (Basel) 2023;13:2158.
27. Pham DT, Nguyen LP, Pham QT, Pham CK, Pham DT, Viet NT, *et al*. A low-cost, flexible extruder for liposomes synthesis and application for murrayafoline a delivery for cancer treatment. J Biomater Appl 2022;37:872-80.
28. Han JY, La Fiandra JN, DeVoe DL. Microfluidic vortex focusing for high throughput synthesis of size-tunable liposomes. Nat Commun 2022;13:6997.
29. Shah A, Patel V, Patel H, Shah D. Development and validation of LC–MS/MS method for pharmacokinetic evaluation of rivastigmine-loaded nanocarriers in rat plasma and brain tissue. J Chromatogr B Analyt Technol Biomed Life Sci 2023;1231:123381.
30. Zhang Y, Li M, Gao X, Chen Y, Liu T. Nanotechnology in neurotherapeutics: Recent development of brain-targeted drug delivery systems. Int J Nanomedicine 2022;17:4105-29.
31. Soni PK, Saini TR. Purification of drug loaded liposomal formulations by a novel stirred cell ultrafiltration technique. Pharm Nanotechnol 2021;9:347-60.
32. Çevikelli T, Yıldız N, Gürsoy RN. Formulation, optimization and *in vitro* evaluation of polymer-coated liposomes encapsulating nebivolol hydrochloride. Int J Polym Mater Polym Biomater 2024;73:897-907.
33. Lehman SE, Benkstein KD, Cleveland TE 4th, Anderson KW, Carrier MJ, Vreeland WN. Particle metrology approach to understanding how storage conditions affect long-term liposome stability. Langmuir 2023;39:12313-23.
34. Hoseini B, Jaafari MR, Golabpour A, Momtazi-Borojeni AA, Karimi M, Eslami S. Application of ensemble machine learning approach to assess the factors affecting size and polydispersity index of liposomal nanoparticles. Sci Rep 2023;13:18012.
35. Pande S. Factors affecting response variables with emphasis on drug release and loading for optimization of liposomes. Artif Cells Nanomed Biotechnol 2024;52:334-44.
36. Sugimoto Y, Suga T, Kato N, Umino M, Yamayoshi A, Mukai H, *et al*. Microfluidic post-insertion method for the efficient preparation of PEGylated liposomes using high functionality and quality lipids. Int J Nanomedicine 2022;17:6675-86.
37. Helms HC, Abbott NJ, Burek M, Cecchelli R, Couraud PO, Deli MA, *et al*. *In vitro* models of the blood-brain barrier: An overview of commonly used brain endothelial cell culture models and guidelines for their use. J Cereb Blood Flow Metab 2016;36:862-90.
38. Liu Y, Zhao Y, Guo D, Zhang M, Li H, Wang T, *et al*. Establishment and characterization of an *in vitro* human blood-brain barrier model based on hCMEC/D3 cells for permeability evaluation. Pharmaceutics 2022;14:1887.
39. Percie Du Sert N, Ahluwalia A, Alam S, Avey MT, Baker M, Browne WJ, *et al*. Reporting animal research:

Explanation and elaboration for the ARRIVE guidelines 2.0. PLoS Biol 2020;18:e3000411.
40. Kuo YC, Chen HH. Surface-engineered PEGylated liposomes with dual targeting and sustained-release characteristics for enhanced brain delivery of therapeutic agents. Int J Pharm 2023;639:122987.
41. Kuo YC, Rajesh R. Pharmacokinetic and pharmacodynamic evaluation of surface-engineered nanocarriers for brain-targeted delivery: Application of non-compartmental analysis and brain targeting indices. Int J Pharm 2022;624:122019.
42. Summerfield SG, Read K, Begley DJ, Obradovic T, Hidalgo IJ, Coggon S, *et al*. Central nervous system drug disposition: The relationship between in situ brain permeability and brain free fraction. J Pharmacol Exp Ther 2022;382:146-58.
43. Stenken JA, Poschenrieder AJ. Bioanalytical chemistry of *in vivo* tissue microdialysis. Anal Chim Acta 2022;1192:339336.
44. Vorhees CV, Williams MT. Assessing spatial learning and memory in rodents using the Morris water maze. Nat Protoc 2022;17:347-76.
45. Giacobini E, Gold G. Alzheimer disease therapy-moving from amyloid-β to tau and cholinergic targets: Assessment of acetylcholinesterase and butyrylcholinesterase activity using Ellman's colorimetric method. Neuropharmacology 2022;210:109030.
46. Pizzino G, Irrera N, Cucinotta M, Pallio G, Mannino F, Arcoraci V, *et al*. Oxidative stress biomarkers in neurodegenerative diseases: Role of malondialdehyde, superoxide dismutase and glutathione in experimental Alzheimer's disease models. Antioxidants 2022;11:1738.
47. Mould DR, Upton RN. Basic concepts in population modeling, simulation, and model-based drug development: Applications to PK/PD modeling and exposure–response analysis in CNS drug delivery. CPT Pharmacometrics Syst Pharmacol 2022;11:1095-112.
48. Motulsky HJ. Intuitive biostatistics in biomedical research: Statistical testing, confidence intervals and multiple comparison approaches in pharmacological studies. Trends Pharmacol Sci 2023;44:315-27.

Source of Support: Nil. **Conflicts of Interest:** None declared.